

# Radio-Loudness of Active Galactic Nuclei: Observational Facts and Theoretical Implications

Marek Sikora<sup>1,2,3</sup>, Lukasz Stawarz<sup>3,4,5</sup>, and Jean-Pierre Lasota<sup>2,4</sup>

<sup>1</sup>*Nicolaus Copernicus Astronomical Center, Bartycka 18, 00-716 Warsaw, Poland*

<sup>2</sup>*Institut d'Astrophysique de Paris, UMR 7095 CNRS, Université Pierre et Marie Curie, 98bis Bd Arago, 75014 Paris, France*

<sup>3</sup>*Kavli Institute for Particle Astrophysics and Cosmology, Stanford University, Stanford CA 94305, and Stanford Linear Accelerator Center, MenloPark CA 94025*

<sup>4</sup>*Astronomical Observatory, Jagiellonian University, ul. Orla 171, 30-244 Kraków, Poland*

<sup>5</sup>*Landessternwarte Heidelberg, Königstuhl, and Max-Planck-Institut für Kernphysik, Saupfercheckweg 1, Heidelberg 69117, Germany*

sikora@camk.edu.pl , stawarz@slac.stanford.edu , lasota@iap.fr

## ABSTRACT

We investigate how the total radio luminosity of AGN-powered radio sources depends on their accretion luminosity and the central black hole mass. Our studies cover about seven orders of magnitude in accretion luminosity (expressed in Eddington units, i.e. as Eddington ratios) and the full range of AGN black hole masses. We find that AGNs form two distinct and well separated sequences on the radio-loudness – Eddington-ratio plane. The ‘upper’ sequence is formed by radio selected AGNs, the ‘lower’ sequence contains mainly optically selected objects. Whereas an apparent ‘gap’ between the two sequences may be an artifact of selection effects, the sequences themselves mark the real upper bounds of radio-loudness of two distinct populations of AGNs: those hosted respectively by elliptical and disk galaxies. Both sequences show the same dependence of the radio-loudness on the Eddington ratio (an increase with decreasing Eddington ratio), which suggests that the normalization of this dependence is determined by the black hole spin. This implies that central black holes in giant elliptical galaxies have (on average) much larger spins than black holes in spiral/disc galaxies. This galaxy-morphology related radio-dichotomy breaks down at high accretion rates where the dominant fraction of luminous quasars hosted by elliptical galaxies is radio quiet. This led to speculations in the literature that formation of powerful jets at high accretion rates is intermittent and related to switches between two disk accretion modes, as directly observed in some BH X-ray binaries. We argue that such intermittency can be reconciled with the spin paradigm, provided that successful formation of relativistic jets by rotating black holes requires collimation by MHD outflows from accretion disks.

*Subject headings:* galaxies: jets – radiation mechanisms: non-thermal – MHD

## 1. Introduction

It took less than two years from the discovery of the first quasars to realize that most of them are radio-quiet rather than radio-loud (Sandage 1965). Strittmatter et al. (1980) pointed out that radio-loudness of quasars, defined as the radio-to-optical flux density ratio, may have a bimodal distribution. Radio bimodality was confirmed by Kellermann et al. (1989), who demonstrated that there are at least 5 – 10 times more radio-quiet than radio-loud quasars (see also Miller, Peacock, & Mead 1990; Stocke et al. 1992). However, most recent studies based on deep radio surveys FIRST and NVSS (Becker, White, & Helfand 1995; Condon et al. 1998), and optical massive surveys SDSS and 2dF (York et al. 2000; Croom et al. 2001), suggest that the bimodality is rather weak, or even may not exist (White et al. 2000; Ivezić et al. 2002; Cirasuolo et al. 2003a,b).

Recently, the issue of radio-loudness got a new dimension: after astronomers had learned how to ‘weight’ supermassive black holes (see Woo & Urry 2002 and refs. therein), it became possible to study the dependence of the radio-loudness parameter,  $\mathcal{R} \equiv L_{\nu_R}/L_{\nu_{opt}}$ , on the Eddington ratio,  $\lambda \equiv L_{bol}/L_{Edd}$ . Here  $L_{\nu_R}$  and  $L_{\nu_{opt}}$  stand for the monochromatic luminosities at some specified radio,  $\nu_R$ , and optical,  $\nu_{opt}$ , frequencies, while  $L_{bol}$  and  $L_{Edd}$  denote the bolometric luminosity of the active nucleus and the appropriate Eddington luminosity ( $L_{Edd} = 4\pi GMm_p c/\sigma_T = 1.3 \times 10^{38} \mathcal{M}/\mathcal{M}_\odot \text{ erg s}^{-1}$ ), respectively. The analysis of radio-loudness for PG quasars, Seyfert galaxies, and LINERS, performed by Ho (2002) seem to indicate that radio-loudness increases with decreasing Eddington ratio, however, with a huge scatter in  $\mathcal{R}$ . His results showed also that the largest  $\mathcal{R}$  are found in AGNs with black hole masses  $\gtrsim 10^8 \mathcal{M}_\odot$ . Such a mass-related duality was recently confirmed by Chiaberge, Capetti, & Macchetto (2005) who included FR I radio-galaxies in their sample. The effect, however, could not be clearly identified for intermediate Eddington ratios. We will show that the reason for the above is that those studies did not take into account luminosities of extended radio structures and did not include broad-line radio galaxies (hereafter BLRGs). These objects are almost exclusively hosted by giant elliptical galaxies and are about  $10^3$  times radio louder than Seyfert galaxies for the same range of the Eddington ratio. The criteria for selection of BLRGs used in our studies are specified in §2. These sources are studied together with Seyfert galaxies, radio-quiet LINERS, FR I radio galaxies, and quasars. The results are presented in §3.

The studies of radio-loudness are crucial for addressing such basic questions as how jets are formed, accelerated and collimated, and why the efficiency of jet production can be so different among objects very similar in all other aspects. The same questions concern jets in black-hole and neutron-star X-ray binaries (XRBs; see review by Fender 2004). Taking advantage of the very short time-scales of XRB variabilities, the dependence of the radio-loudness on the Eddington ratio in these objects can be traced directly, for each source individually. Such studies indicate that at low luminosities the radio-loudness is a monotonic function of the accretion luminosity (Gallo, Fender & Pooley 2003), while at the highest luminosities it may jump by a large factor, following transitions between two accretion states (Fender, Belloni, & Gallo 2004). If the radio activity of individual AGNs depends on the Eddington ratio in a similar way, then the observed huge differences of radio-loudness for AGNs with similar Eddington ratio, especially at its lowest values, indicates

that yet another parameter in addition to the accretion rate must play a role in determining the jet production efficiency. In §4 we investigate the possibility that this parameter is the black-hole spin and speculate how the spin paradigm can be reconciled with intermittent jet activity at higher accretion rates. Our main results and their theoretical implications are summarized in §5.

In this paper we assume  $\Lambda$ CDM cosmology, with  $\Omega_M = 0.3$ ,  $\Omega_\Lambda = 0.7$ , and the Hubble constant  $H_0 = 70 \text{ km s}^{-1} \text{ Mpc}^{-1}$ .

## 2. Samples

Our studies include: radio-loud broad-line AGNs (BLRGs plus radio-loud quasars); Seyfert galaxies and LINERS; FR I radio galaxies; optically selected quasars. The subsamples were selected according to the following criteria:

- the optical flux of the central, unresolved source is known;
- the total radio flux is known (including extended emission if present);
- black hole masses or necessary parameters to estimate them are available in literature.

Other criteria, applied individually to different subsamples, are specified below. In our sample, we did not include blazars, i.e., OVV-quasars, HP-quasars, and BL Lac objects, because their observed emission is significantly Doppler boosted. We also did not analyze narrow line radio galaxies (NRLGs), because their optical nuclei are hidden by “dusty tori”, which makes estimation of the accretion rates very uncertain.

### 2.1. Radio-selected broad line AGN

The objects are taken from Eracleous & Halpern (1994; 2003; hereafter EH94 and EH03, respectively) who studied profiles of the broad  $H\alpha$  emission lines of radio-loud AGNs with  $z \leq 0.4$ , selected from Véron-Cetti & Véron (1989). We divided the sample in two sub-groups: the radio-loud quasars and BLRGs, with the commonly used division line at  $M_V = -23$  which corresponds to the  $V$ -band luminosity  $L_V \simeq 10^{44.6} \text{ ergs s}^{-1}$ . They are listed in Tables 1 and 2, along with the following data: IAU coordinates for the J2000.0 epoch; name of the source; redshift,  $z$ , with the most accurate values taken from Eracleous & Halpern (2004);  $V$ -band total apparent magnitude,  $m_V$ , taken from EH94 and EH03; Galactic extinction,  $A_V$ , available in NED (<http://nedwww.ipac.caltech.edu/>); starlight contamination,  $\kappa_*$ , taken from EH94 and EH03; total radio flux at  $\nu_5 \equiv 5 \text{ GHz}$ ,  $F_5$ , obtained from the literature with references provided in the tables; FWHM of the  $H\alpha$  line taken from EH94 and EH03. We have used these data to calculate other quantities included in the tables, namely: the optical luminosity of the nucleus at  $\lambda_B \equiv 4400\text{\AA}$ ,  $L_B \equiv \nu_B L_{\nu_B}$ ; the radio luminosity at

5 GHz,  $L_R \equiv \nu_5 L_{\nu_5}$ ; the radio-loudness parameter,  $\mathcal{R} \equiv L_{\nu_5}/L_{\nu_B} = 1.36 \times 10^5 (L_R/L_B)$ ; the black hole mass,  $\mathcal{M}_{\text{BH}}$ ; and finally the  $L_B$  and  $L_R$  luminosities expressed in the Eddington units.

The  $B$ -band nuclear luminosity was calculated using the standard luminosity-flux relation:

$$L_B = 4\pi d_L^2 \nu_B F_{\nu_B} (1+z)^{-(1-\alpha_{opt})} \quad , \quad (1)$$

where  $d_L$  is the luminosity distance calculated for a given redshift and the assumed cosmology,  $\alpha_{opt}$  is the power-law slope around  $\nu_B$ , and the  $B$ -band nuclear flux is

$$\nu_B F_{\nu_B} = (\lambda_V/\lambda_B)^{(1-\alpha_{opt})} [-0.4(m_V - A_V) - 4.68] (1 - \kappa_*) \quad , \quad (2)$$

where  $\lambda_V \equiv 5500\text{\AA}$ , and  $\alpha_{opt} = 0.5$  is taken. In this paper we also assume the bolometric luminosity of the active nucleus  $L_{bol} = 10 L_B$ . The total radio luminosity of the source,  $L_R$ , was evaluated using a formula analogous to the one given by Eq.(1), with the assumed radio spectral index  $\alpha_R = 0.8$  for the K-correction. We note, that most of the objects in this subsample are strong radio sources ( $F_5 > 0.03$  Jy), have radio-morphologies of the FR II type and radio luminosities dominated by the extended structures. Radio fluxes for most of them were therefore taken from the single-dish radio surveys (Wright & Otrupcek 1990, Gregory & Condon 1991). In the case of the three weak sources IRAS 02366-3101, MS 0450.3-1817, and CBS 74, for which the radio data from other facilities were used as indicated in the tables, the provided radio fluxes (and hence  $L_R$  and  $\mathcal{R}$  parameters) should be rather considered as lower limits. Finally, since black hole masses for most of the Eracleous and Halpern objects are not available in literature, we estimated them using a BLR size–luminosity relation assuming virial velocities of the gas which produces broad  $\text{H}\alpha$  lines (see, e.g., Woo & Urry 2002 and references therein),

$$\frac{\mathcal{M}_{\text{BH}}}{\mathcal{M}_{\odot}} = 4.8 \times \left[ \frac{\lambda L_{\lambda}(5100\text{\AA})}{10^{44} \text{ergs/s}} \right]^{0.7} \text{FWHM}_{\text{H}\alpha}^2 \quad , \quad (3)$$

where  $\text{FWHM}_{\text{H}\alpha}$  is derived by EH94 or EH03, and  $L_{\lambda}(5100\text{\AA}) = (\lambda_B/5100\text{\AA})^{(1-\alpha_{opt})} L_B$ .

## 2.2. Seyfert galaxies and LINERS

This sample contains objects selected from Ho & Peng (2001) and Ho (2002; hereafter HP01 and H02, respectively). All objects studied by HP01 have Seyfert 1 type nuclei and are taken from the Palomar and CfA surveys. We selected only those for which estimations of black hole masses were available in literature. The sample of H02 is composed by AGNs with given black hole masses and includes Seyfert galaxies, LINERS, Transients, and PG quasars. We included only AGNs for which at least the  $\text{H}\alpha$  line is broad, i.e., we did not include galaxies with nuclei of spectral type S2, L2, and T2. We did not include here PG quasars — they are treated by us separately (see §2.4). The final ‘Seyferts + LINERS’ sample is made from 39 objects (36 galaxies with Seyfert nuclei and 3 LINERS) listed in Table 3. The table encloses information about IAU coordinates for the

J2000.0 epoch; name of the source; distance of the source,  $d$ ; absolute  $B$ -magnitude of the nucleus,  $M_B$ ;  $B$ -band luminosity of the nucleus,  $L_B$ ; total radio luminosity at 5 GHz,  $L_R$ ; radio-loudness parameter,  $\mathcal{R}$ ; black hole mass,  $\mathcal{M}_{\text{BH}}$ , followed by the appropriate reference; and finally the  $B$ -band and radio luminosities in the Eddington units.

Distances, if less than 40 Mpc ( $z < 0.009$ ), are the same as adopted by H02 from Tully (1988). They were derived taking into account the effect of the Virgo infall. If larger, the values given in H02 were multiplied by a factor (0.75/0.7), due to the difference in the value of the Hubble constant used in H02 and in this paper. Absolute  $B$ -magnitudes of nuclei,  $M_B$ , were taken from HP01 if available. These are the values calculated from directly measured apparent magnitudes  $m_B$  of the nuclear regions. In other cases,  $M_B$  were taken from H02. These are obtained from the  $L_{H\beta} - M_B$  correlation. For distances to the source larger than 40 Mpc, the absolute magnitude  $|M_B|$  was increased by a factor  $(2.5 \log[0.75/0.7]^2)$ . The nuclear luminosity,  $L_B$ , was then calculated from the absolute  $B$ -magnitude,  $M_B$ , using the standard relation

$$\log L_B = 0.4|M_B| + 35.6 \quad . \quad (4)$$

Regarding the radio emission, contrary to HP01 and H02, we decided to use in our studies of the AGN radio-loudness the total luminosities, i.e. including nuclear and extended emission (see §3.4). The total radio luminosities are taken from H02 and HP01 and as the optical luminosities they are corrected to account for different values of the Hubble constant.

### 2.3. FR I radio galaxies

Our sample of FRI radio galaxies consists of objects which were observed by Hubble Space Telescope and hence have determined optical luminosities (or the appropriate upper limits) for their unresolved cores (see Kharb & Shastri 2004, and references therein) and in addition estimated black hole masses (Cao & Rawlings 2004; Woo & Urry 2002). Such sample contains 31 objects listed in Table 4 along with the optical and radio data: the IAU coordinates for the J2000.0 epoch; name; redshift,  $z$ ;  $B$ -band luminosity  $L_B$ , obtained after recalculating  $V$ -band luminosities provided by Kharb & Shastri (2004) to the cosmology we are using and then converted to  $B$ -band assuming optical spectral index  $\alpha_{opt} = 0.5$ ; total radio flux at 5 GHz,  $F_5$ , obtained from the literature indicated in the table (and if originally provided at other frequencies, recalculated assuming radio spectral index  $\alpha_R = 0.8$ ); total 5 GHz radio luminosity,  $L_R$ ; radio-loudness parameter,  $\mathcal{R}$  (assuming that the accretion luminosity is equal to the one observed from the optical core by HST); black hole mass,  $\mathcal{M}_{\text{BH}}$ , taken from Woo & Urry (2002) and Cao & Rawlings (2004); and finally  $B$ -band and radio luminosities expressed in the Eddington units.

## 2.4. PG quasars

This sample consists of those BQS objects (Schmidt & Green 1983) which have redshifts less than  $z = 0.5$ , black hole mass available in literature, and are not included in our other sub-samples. The BQS objects are commonly called PG (Palomar-Green) quasars, despite the fact that not all of them satisfy the formal luminosity criterion  $M_V$  or  $M_B < -23$  to be classified as quasars (there are 7 of such BQS AGNs in our sample). The sample is listed in Table 5, along with the optical and radio data: the IAU coordinates for the J2000.0 epoch; name; redshift,  $z$ ;  $B$ -band luminosity  $L_B$ , calculated for  $m_B$  given by Schmidt & Green (1983);  $F_5$ , obtained from Kellerman et al. (1989); total 5 GHz radio luminosity,  $L_R$ ; radio-loudness parameter,  $\mathcal{R}$ ; black hole mass,  $\mathcal{M}_{\text{BH}}$ , taken from Vestergaard (2002) or Woo & Urry (2002); and finally  $B$ -band and radio luminosities expressed in the Eddington units.

## 3. Results

### 3.1. Global patterns

Radio luminosities vs. optical luminosities of the selected AGNs are plotted in Figure 1. As can be seen our sub-samples form two sequences which are separated by  $\sim 3$  orders of magnitude in radio luminosity. One can check from Tables 1-5, that the upper sequence is almost exclusively populated by objects with black hole masses  $\mathcal{M}_{\text{BH}} > 10^8 \mathcal{M}_{\odot}$ . The only exception one object from the ‘Seyferts plus LINERS’ sub-sample, NGC 1275. It should be noted, however, that this object, as all the other AGNs in the upper sequence, is hosted by a giant elliptical galaxy (specifically, by the cD galaxy of the Perseus cluster), and has an extended FR I-like radio structure observed presumably at a small angle to the line of sight (Pedlar et al. 1990). Close to the upper sequence but still belonging to the ‘Seyferts plus LINERS’ subsample is located NGC 4258 (M106). This spiral galaxy hosts an extremely weak AGN. Its total radio luminosity is about 100 times larger than the nuclear one, and most likely is not related to the jet activity.

Whereas there are no disc-galaxy-hosted AGNs in the upper sequence, AGNs hosted by giant elliptical galaxies are present in both the upper and lower sequences. This particularly concerns highest accretion luminosity objects, i.e. quasars. Most of them in fact, even those with very massive black holes and resolved elliptical hosts, occupy the lower sequence which we will call hereafter the ‘radio-quiet sequence’(see §4.1). At intermediate accretion luminosities, AGNs hosted by giant elliptical galaxies and located in the lower sequence are represented in our sample only by four objects. However, recent discoveries of many radio-quiet galaxies with very broad Balmer lines and hosting very massive black holes (Strateva et al. 2003; Wu & Liu 2004) strongly indicate that rareness of such objects in the Eracleous & Halpern samples might be due only to selection effects. Hence, it is plausible that also at intermediate accretion luminosities, most of AGNs hosted by giant elliptical galaxies are radio-quiet.

An intriguing feature of the Figure 1 is that both the radio-quiet sequence and the ‘radio-loud’ upper sequence have a similar dependence of radio-luminosity on the accretion-luminosity. It corresponds to an approximate constancy of  $L_R$  at larger values of  $L_B$  and to a decrease of  $L_R$  at smaller accretion rates. As shown in Figure 2, qualitatively the same feature is found when luminosities are expressed in Eddington units. The main difference between Figures 1 and 2 is the relative location of the two sequences which reflect the fact that AGN black-holes in the radio-loud sequence are on average  $\sim 20$  times more massive than black holes in the AGNs forming the radio-quiet sequence. In Figure 2 this causes a left-down shift of the upper sequence relative to the lower sequence. Obviously due to a wide range of black hole masses in each of the sequences there are quantitative differences in the location of individual objects within the sub-samples. Furthermore, at the largest accretion luminosities, where the lower pattern is occupied mostly by quasars hosted by giant elliptical galaxies, the relative location of the two sequence is not significantly modified.

In Figure 3, we plot the dependence of the radio-loudness,  $\mathcal{R}$ , on the Eddington ratio,  $\lambda$ , assuming  $\lambda = L_{bol}/L_{Edd} = 10(L_B/L_{Edd})$  (see, e.g., Richards et al. 2006).<sup>1</sup> Our results confirm the trend of the increase of radio-loudness with decreasing Eddington ratio, originally noticed by Ho (2002; see also Merloni, Heinz, & Di Matteo 2003; Nagar, Falcke, & Wilson 2005). However, we show in addition that this trend is followed separately — with a large difference in normalization — by the ‘radio-quiet’ and the ‘radio-loud’ sequences. Yet another feature revealed in Figure 3 is a clear change of slope of the  $\mathcal{R} - \lambda$  dependence indicating some sort of saturation of radio-loudness at low Eddington ratios. A similar trend can be noticed, but specifically for FR I and FR II radio galaxies, in the data presented by Zirbel & Baum (1995). Let us recall that almost all BLRGs and radio-loud quasars in our samples have FR II radio morphology.

Finally, in Figure 4 we illustrate the dependence of radio-loudness on black-hole mass. This plot demonstrates that AGNs with the black hole masses  $> 10^8 \mathcal{M}_\odot$  reach values of radio-loudness three orders of magnitude larger than AGNs with black hole masses  $< 3 \times 10^7 \mathcal{M}_\odot$ . A relatively smooth transition between those two populations most likely is caused by the overlap between black hole masses hosted by disc and elliptical galaxies. Errors in black hole mass estimations can also have a similar effect. It is interesting to compare our Figure 4 with the analogous figures restricted to high Eddington-ratio objects presented by Laor (2003) and McLure & Jarvis (2004). One can see that in all cases there is a difference of about 3 orders of magnitude between the maximal radio-loudness of AGNs with  $\mathcal{M}_{BH}/\mathcal{M}_\odot > 10^8$  and AGNs with less massive black holes. However, because in our sample we have included AGNs with very low Eddington-ratios the boundaries of maximal radio-loudness for less and more massive objects are now located at much larger  $\mathcal{R}$ . This effect is a simple consequence of the radio-loudness increasing with decreasing Eddington-ratio. Because of this, the upper radio boundaries are determined by low- $\lambda$  objects: in the lower- $\mathcal{M}_{BH}$

---

<sup>1</sup>Note that for very low luminosity AGNs the bolometric correction can be a factor  $\sim 2$  larger than considered above. However, due to very large uncertainties and not known functional dependence of the exact correction factor on the luminosity (Ho 1999), we decided to use the same proportionality constant for all the analyzed AGNs.

sub-group by Seyferts and LINERS, in the larger- $\mathcal{M}_{\text{BH}}$  sub-group by FR Is.

### 3.2. Incompleteness of our sample and related uncertainties

Our sample is very heterogeneous, being composed from incomplete sub-samples selected using different criteria. This must have effects on the presented plots and should be taken into account when interpreting our results. The largest incompleteness concerns the broad-line AGNs taken from the radio-selected samples. They include BLRGs and radio-loud quasars, which are all associated with giant elliptical galaxies. However, as known from radio studies of optically selected quasars, the majority of such sources are radio-quiet and many are radio-intermediate (White et al. 2000). The same was recently found for lower- $\lambda$  objects, when investigating the double-peaked broad emission lines in AGNs from the SDSS catalog (Strateva et al. 2003). Contrary to the deeply grounded conviction that the presence of double-peaked lines is unique to BLRGs, it was discovered that such lines are pretty common also in radio-quiet AGNs with black hole masses characteristic of giant elliptical galaxies (Wu & Liu 2004). Noting all that, one should consider the upper, radio-loud sequence in our plots as populated only by a minority of the elliptical-hosted AGNs. In other words, with a complete (though not yet available) sample, the mid-Eddington AGNs in giant elliptical galaxies would not be confined to the upper sequence, but would show continuous distribution down to the lowest detectable radio levels, similarly to the PG quasars in our sample.

Meanwhile, the results presented by Wu & Liu (2004) in the right panels of their Figure 1 seem to indicate that for  $\lambda < 10^{-3}$  the proportions between radio-loud and radio-quiet fractions discussed above can reverse, i.e., that for  $\lambda < 10^{-3}$  the upper sequence is populated by the majority of the elliptical-hosted AGNs. This seems to be confirmed by relatively complete surveys of nearby galaxies, for which the prospect of missing radio-quiet AGNs among giant elliptical galaxies is rather low (see, e.g., Terashima & Wilson 2005, Chiaberge et al. 2005).

Finally, our sample is incomplete also because it does not include narrow-line Seyferts 1 (NLS1). These objects are presumably hosted by disc galaxies and represent high accretion-rate AGNs with relatively low black hole masses. They are radio-quiet as a class (Ulvestad, Antonucci, & Goodrich 1995), with only a few reaching  $\mathcal{R} > 100$ , and none producing a prominent extended radio structure (Zhou & Wang 2002; Whalen et al. 2006; Komossa et al. 2006). If included in our plots, they would form extension of the lower, radio-quiet pattern to large  $\lambda$ 's.

### 3.3. Potential errors and attempts to minimize them

Some quantities used to construct our plots can be subject to significant errors. This primarily concerns galaxies with very weak nuclei. Sometimes it is even difficult to decide whether the observed nuclear features are dominated by the AGN or by starburst activities, and thus what is the real accretion luminosity. To avoid the impact of such uncertainties on our results we did not



include in the ‘Seyferts + LINERS’ sample objects of spectral type 2, i.e. those with no broad lines. On the other hand, uncertainties concern also sources with broad-line nuclei, firstly because of the accretion-luminosity contamination by starlight, and secondly because of the internal extinction. To avoid these uncertainties, Ho (2002) calculated accretion luminosities indirectly, using the correlation of the accretion luminosity (or more precisely – absolute magnitude  $M_B$ ) with the intensity of the  $H\beta$  line. However, as one can see in Ho & Peng (2001), this correlation is reasonable only for very luminous objects. Therefore, to minimize the related uncertainties, for sources overlapped by samples from Ho & Peng (2001) and Ho (2002), we adopted nuclear luminosities obtained in Ho & Peng from the direct optical measurements and corrected by subtracting the starlight.

Our selection of FR I radio-galaxies is less rigorous: in this subsample we included also the objects for which there are no direct signatures of an accretion flow. We note that the correlation between the optical fluxes of the nuclear cores observed in these sources by the HST and their radio fluxes suggests that the observed nuclear emission is due to synchrotron radiation originating in the inner portions of the jets (Verdoes Kleijn, Baum, & de Zeeuw 2002). Hence, in several papers it was assumed that HST detections provide the upper limits for the optical radiation due to the accretion flow (see, e.g., Chiaberge, Capetti, & Celotti 1999; Chiaberge, Capetti, & Macchetto 2005). However, it does not have to be the case if the central nuclei are hidden by “dusty tori”. Then the situation might be the opposite: the accretion luminosity can be in fact larger than the luminosity measured by HST. Arguments in favor of such a possibility were put forward by Cao & Rawlings (2004), who postulated that indeed BL Lac objects accrete at the high rates. There are, however, strict limits on the bolometric luminosity of hidden AGN: it cannot be larger than the observed infrared luminosity resulting from reprocessing of the hidden nuclear radiation by the circumnuclear dust. Infrared observations clearly indicate that active cores in FR I’s radiate several orders of magnitude below the Eddington level (Knapp, Bies, & van Gorkom 1990; Müller et al. 2004; Haas et al. 2004). By comparing the infrared luminosities with the HST measurements for a number of FR I radio galaxies included in our sample, we find that the accretion luminosities of some of them might be underestimated by a factor larger than 10.

Other errors which may significantly affect details of our plots come from the estimations of black-hole masses. For all the objects except BLRGs and radio-loud quasars, these masses were taken from the literature. They were obtained using variety of methods. However, by comparing Figure 1 and 2, which are constructed with and without involving black hole masses, respectively, one can see that such global features as two-sequence structure and the general trends survive. Hence we conclude that our results are not significantly affected by errors of black-hole mass estimations.

Finally, we should comment on our choice of calculating the radio-loudness parameter by using not the strictly nuclear radio fluxes (as in several other similar studies) but the total ones. In the cases of lobe-dominated radio quasars, BLRGs, and FR I radio galaxies, the observed radio luminosity is produced mainly by the jet-powered extended radio structures. As long as our interest in radio-loudness is to understand the strong diversity of the jet power, the extended radio com-

ponent should be therefore considered. Less obvious is the situation in the case of AGNs hosted by spiral galaxies. There the nuclear radio emission is usually dominant while the extended radio emission can be due not only to jet activity, but also to starburst regions. Hence by using total radio fluxes, as we did in this paper, one can overestimate radio-loudness (which should concern only the jet-related emission). Such a choice is however more appropriate than taking into account only the nuclear radio component: in this way we avoid underestimating the radio-loudness, which would artificially increase the gap between the upper and lower patterns in Figures 1-3. In other words, our choice is conservative.

## 4. Discussion

### 4.1. Radio-loudness vs. galaxy morphology

Using several subsamples of AGNs which together cover seven decades in the Eddington ratio, we have demonstrated that radio-selected AGNs hosted by giant elliptical galaxies can be about  $10^3$  times radio louder than AGNs hosted by disc galaxies, and that the sequences formed by the two populations show the same trend — an increase of the radio-loudness with the decrease of the Eddington ratio. This corresponds to a slower than linear decrease of the (Eddington-scaled) radio luminosity with the decrease of the Eddington-ratio. The same trend was discovered by Ho (2002), but because his paper considered only nuclear radio luminosities and didn't include BLRG, the radio-loudness vs. Eddington-ratio plot did not reveal a double-sequence structure. A trend similar to ours was found also by Terashima & Wilson (2003), but in the plane 'radio-loudness vs. X-ray luminosity', where radio-loudness is defined as the ratio of the radio to the X-ray luminosity. These authors considered two cases, one with radio-loudness including only nuclear radio luminosities and another with radio-loudness defined for the total radio luminosity. In the latter case, in similarity to our results, a double-sequence structure emerges. A double-sequence structure was noticed also by Xu, Livio & Baum (1999), in the 'radio-luminosity vs. [OIII] luminosity' plane. These results strongly confirm that when one considers the total radio luminosity, AGNs split into two subclasses, with AGNs hosted by giant ellipticals extending to much larger radio luminosities than AGNs hosted by disk galaxies. It is the consequence of the fact that radio-galaxies have powerful extended radio-emission that must be obviously taken into account when estimating their radio fluxes.

The absence of prominent, extended radio structures in AGNs hosted by disc galaxies, when confronted with giant elliptical hosts of the classical double radio sources, led in the past to the conviction that all AGNs in disc galaxies are radio-quiet, and that all AGNs in giant elliptical galaxies are radio-loud. Only recently, after the HST allowed to image and determine the host morphologies of distant, luminous quasars, it has become clear that the claimed one-to-one correspondence between the radio-loudness and the galaxy morphology is invalid: a number of luminous, radio-quiet quasars have been found to be hosted by giant elliptical galaxies (see Floyd et al. 2004

and references therein). This discovery stimulated in turn searches for radio-loud AGNs among those hosted by disc galaxies. Surely, Ho & Peng (2001) demonstrated that after subtraction of the starlight, nuclei of some Seyfert galaxies ‘become’ radio-loud, according to criterion  $\mathcal{R} > 10$  introduced by Kellerman (1989) for quasars. The same was found for LINERS in nearby disc galaxies (Ho 2002). However, as we have shown in this paper, all Seyfert galaxies and LINERS remain well separated from the BLRGs and FR I radio galaxies, and the fact that some of them reach  $\mathcal{R} > 10$  is caused by the increase of the radio-loudness with the decreasing  $\lambda$ .

#### 4.2. Two sequences imply two parameters; comparison with BH X-ray binaries

Comparing observed properties of AGN to those of radio active black-hole X-ray binaries provides important hints about the nature (assumed to be common) of the jet production mechanism in these two classes of objects. Gallo, Fender, & Pooley (2003) discovered that radio luminosities of BH binaries in low/hard states (i.e., at low accretion rates) correlate with X-ray luminosities,  $L_X$ . They found that luminosity variations of two objects, GX 339-4 and V404 Cyg, follow the relation  $L_R \propto L_X^{0.7}$  which holds over more than three order of magnitudes in  $L_X$  with the same normalization within a factor of 2.5. This discovery triggered speculations that the powering of radio activity in XRBs during the low/hard state is entirely determined by accretion. However, the fact that a similar trend, albeit with a huge scatter, is followed by both our AGN sequences (compare the low- $L_B/L_{\text{Edd}}$  sections in our Figure 2 with Figure 2 from Gallo et al. [2003]) shows that radio-loudness cannot depend only on the accretion rate: clearly an additional parameter is required to explain the bimodal distribution of radio-loudness for spiral-hosted and elliptical-hosted AGNs at low  $\lambda$ 's, and its significant scatter within both sequences.

The monotonic dependence of radio luminosities on the Eddington ratio in XRBs breaks down at  $\lambda \sim 0.01$ , and observations clearly indicate the intermittency of the jet production at higher luminosities and its connection with a spectral state (Fender, Belloni, & Gallo 2004). Qualitatively a similar break but located at smaller  $\lambda$ 's is seen in the AGN sequences.

Motivated by the similarities of the low- and high- $\lambda$  patterns in XRBs and AGNs, Merloni, Heinz, & Di Matteo (2003) proposed that at high accretion luminosities the jet production is intermittent also in AGNs. This idea was recently explored and supported by Nipoti, Blundell, & Binney (2005). However, at high accretion rates (just as at the low ones discussed previously) spiral-hosted AGNs are located exclusively in the radio-quiet sequence of our Figures 1-3, as opposed to quasars which populate both upper and lower patterns. Only few exceptional cases are known in which the high- $\lambda$  spiral-hosted AGNs reach radio-loudness  $\mathcal{R} > 100$  (Véron-Cetti & Véron 2001; Ledlow et al. 2001; Whalen et al. 2006) — all the other objects of this kind are  $\sim 10^3$  times radio weaker than the radio-loud quasars and BLRGs with similar values of  $\lambda$ . Clearly this fact indicates again that an additional parameter must play a role in explaining why the upper, radio-loud sequence in Figures 1-3 is reachable only by the AGNs hosted by early type galaxies.

### 4.3. The spin paradigm

It is natural to expect that the second (in addition to accretion rate) physical parameter determining radio-loudness of AGNs is related to the properties of the central black-hole. In this case we are left with only two possibilities: mass and spin. Although the upper sequence is formed by massive black-holes only, the mass cannot be the required physical parameter unless one invents a specially designed mass-scaled jet launching mechanism. The black-hole mass, however, reflects the history of its growth and in this fashion is related to both the galaxy’s morphology and to the other parameter: the spin. In the next section we will show how the black-hole’s spin can explain the radio-loudness “bimodality” but since this idea has a rather long and eventful history, we will first review shortly the past and present-day status of the so-called ‘spin paradigm’.

In 1990, Blandford suggested that efficiency of the jet production (assuming that a jet is powered by the rotating black hole via the Blandford-Znajek (1977) mechanism) is determined by the black hole spin,  $J$ , or, more precisely, by the dimensionless angular momentum,  $a \equiv J/J_{max} = cJ/GM_{BH}^2$ . This is a very attractive because in principle it can explain the very wide range of radio-loudness of AGNs that look very similar in many other aspects. This spin paradigm was explored by Wilson & Colbert (1995) and Hughes & Blandford (2003), who assumed that the spin evolution is determined by black-hole mergers. They showed that mergers of black holes which follow mergers of galaxies lead to a broad, ‘bottom-heavy’ distribution of the spin, consistent with a distribution of radio-loudness in quasars. As shown by Moderski & Sikora (1996a,b) and Moderski, Sikora & Lasota (1998), ‘bottom-heavy’ distribution of the spin is reachable also if the evolution of the black hole spin is dominated by accretion, provided the accretion history consists of many small accretion events with randomly oriented angular momentum vectors. In such a case, accretion events lead to formation of both co-rotating and counter-rotating discs depending on the initial angular momenta, which in turn spin-up and spin-down the black hole. This possibility was questioned by Natarajan & Pringle (1998) and Volonteri et al. (2005) who argued that angular momentum coupling between black holes and accretion discs is so strong, that the innermost portions of a disc are always forced to co-rotate with a black hole, and therefore all AGN black-holes should have large spins. However, as was demonstrated by King et al. (2005) and confirmed by Lodato & Pringle (2006), counter-rotating disks can in fact be formed, provided individual accretion events involve much smaller amount of material than the mass of the black hole.

### 4.4. The revised spin paradigm

Our new, revised version of the spin “paradigm”, based on the existence of two radio-loudness sequences, states that the radio-loud, upper-sequence AGNs have high black-hole spins. This version of the spin (or rather “spin-accretion”) paradigm must be completed by two elements:

- (I). Black hole evolution scenarios explaining why the spin distribution of BHs hosted by giant

elliptical galaxies extends to much larger values than in the case of spiral galaxies;

- (II). A spin-accretion scenario explaining the intermittent jet activity at high accretion rates.

We will discuss the evolution problem first, but before that let us just mention that in black-hole XRBs the situation is simpler: since to reach the maximum spin a black hole has to double its mass, black-hole spins in low-mass binaries do not evolve during the lifetime of the systems. Therefore one should not expect in this case the presence of two radio-loudness sequences as observed (Gallo et al. 2003). Observations suggest ‘moderate’ black-hole spin values in several XRBs (see e.g. Shafee et al. 2006 and Davis, Done & Blaes 2006) so in principle they would be equivalent to the “radio-loud” AGN sequence.

#### 4.4.1. Black-hole spin-up

The spin-up of BHs in spiral galaxies can be limited by multiple accretion events with random orientation of angular momentum vectors, and small increments of accreted mass

$$m \ll m_{align} \sim a \sqrt{\frac{R_S}{R_w}} \mathcal{M}_{BH} \quad , \quad (5)$$

where  $R_S = 2GM/c^2$  is the Schwarzschild radius and  $R_w (\sim 10^4 R_g)$  is the distance of the warp produced by the Bardeen-Petterson process in the accretion disk, which at large distances is inclined to the equatorial plane of the rotating black hole (Bardeen & Petterson 1975)<sup>2</sup>. Only with such small increments of accreting mass, a counter-rotating accretion disk can survive over a whole accretion event, as otherwise it would undergo a flip due to an alignment process which tends to co-align a BH angular momentum with an angular momentum of the distant ( $R \geq R_w$ ) regions of the accretion disk (Rees 1978). The accretion-event mass limit (Eq. 5) is severe but consistent with observations indicating very short life-times of individual accretion events in Seyfert galaxies (Capetti et al. 1999; Kharb et al. 2006) and showing a random orientation of jets relative to the host galaxy axis (Kinney et al. 2000; Schmitt et al. 2001). It should be also noted that fueling of AGN in disk galaxies is presumably not related to the galaxy mergers and is provided by molecular clouds (Hopkins and Hernquist 2006). Alternatively, the low values of spins of BHs in disk galaxies could be assured if the BH growth is dominated by mergers with intermediate mass BHs — relics of Population III stars or BHs formed in young stellar clusters (see Mapelli, Ferrara, & Rea 2006 and refs. therein).

---

<sup>2</sup>The required mass increments may be even smaller, if the viscosity related to the ‘vertical’ shear is larger than viscosity related to the ‘planar’ shear and when the angular momentum of the warped disk is smaller than the angular momentum of the black hole (Papaloizou & Pringle 1983; Natarajan & Pringle 1998; see however discussion in King et al. 2005, Sect. 4.2).

In contrast to spiral galaxies, giant ellipticals underwent at least one major merger in the past (see, e.g., Hopkins et al. 2006). Such mergers are followed by accretion events which involve too much mass to satisfy the condition given by Eq.(5). Then, regardless of whether the disk was initially counter- or co-rotating, due to the alignment process, all disks will co-rotate (counter-rotating disks undergo flips). Provided that  $m \gg m_{align}$  they spin-up black holes to large values of  $a$ , up to  $a > 0.9$  if  $m \sim M_{BH}$ . This is in agreement with the large average spin of quasars as inferred from comparison between the local BH mass density and the amount of radiation produced by luminous quasars (Soltan 1982; Yu & Tremaine 2002; Elvis, Risasli, & Zamorani 2002; Marconi et al. 2004). This explains why AGNs on the upper branch have high spins in full agreement with our version of the spin paradigm. However, since most quasars are radio-quiet (a “bottom-heavy” distribution of radio-loudness), the version of the spin paradigm according to which the distribution of the radio-loudness of quasars matches the distribution of their spin is invalidated. This brings us to the second problem: the intermittent jet activity at high accretion rates.

#### 4.4.2. Intermittency

Despite the “bottom heavy” distribution of quasar radio-loudness one can still consider the spin to be the parameter which determines the power of an outflow. However, such an outflow may fail to become a jet unless it is collimated (Begelman & Li 1994). Hence, we suggest that the intermittent production of narrow jets, as seen directly in XRBs, is related to intermittent collimation and that the latter is provided by a surrounding non-relativistic MHD outflow launched in the accretion disc. Such a double jet structure was originally proposed by Sol, Pelletier, & Asseo (1989), and shown to provide good collimation by Bogovalov & Tsinganos (2005), Gracia, Tsinganos, & Bogovalov (2005), and Beskin & Nokhrina (2006). Assuming that at high accretion rates the disc has two realizations, being driven by viscous forces or by magnetic torques from MHD winds, one can obtain intermittency of collimation by transitions between two such accretion modes. As Livio, Pringle, & King (2003) suggested and Mayer & Pringle (2006) confirmed, such transitions can be governed by processes responsible for generation of a poloidal magnetic field. An alternative scenario, proposed by Spruit & Uzdensky (2005), involves a drift of isolated patches of magnetic fields to the center from very large distances.

At low  $\lambda$ 's intermittency is not observed (or rather it is not deduced from observations) and as mentioned in Sect. 3.2 a “top heavy” distribution of radio-loudness for ellipticals is there emerging.

#### 4.5. Other challenges?

The spin paradigm may be challenged by the following observations:

- (i). the very large spin of the central black-hole in the radio-quiet Seyfert galaxy MCG-6-30-15

deduced from the profile of the fluorescent iron line (Wilms et al. 2001);

- (ii). the significant content of protons in quasar jets, as deduced from the analysis of blazar spectra (Sikora & Madejski 2000; Sikora et al. 2005), and indicated by the discovery of circular polarization in radio cores (Wardle et al. 1998; Homan, Attridge, & Wardle (2001);
- (iii). the presence of relativistic jets in the neutron star XRBs (Fomalont, Geldzahler & Bradshaw 2001; Fender et al. 2004).

Can the spin paradigm be reconciled with these features?

*(i) The Seyfert galaxy MCG 6-30-15:* The interpretation of the very extended and weak red wing of the fluorescent iron line observed in the radio-quiet Seyfert galaxy MCG 6-30-15 in terms of the model involving rapid rotation of the central black hole (Wilms et al. 2001) is not unique, and depends crucially on the details of the continuum production in the vicinity of the black hole. These details are very uncertain (Beckwith & Done 2004). Furthermore, broad fluorescent iron lines can be produced also in the wind (Done & Gierliński 2006). Finally, morphology of the host galaxy is E or SO (Ferruit, Wilson, & Mulchaey, 2000) and therefore the object could have undergone a major merger. In addition, McHardy et al (2005) found  $\lambda \approx 0.4$  for this object. Hence, MCG 6-30-15 may indeed harbor a rapidly spinning black hole, but as most *quasars*, it happens to be observed in its radio quiet state.

*(ii) Protons in quasar jets:* Theories of jet launching by rotating black holes predict a zero proton content (see particular models by Hawley & Krolik 2006; McKinney 2006; and refs. therein). This is because proton loading near the black hole is protected by the magnetic fields threading the horizon (note that the Larmor radius of non-relativistic protons is many orders of magnitude smaller than the size of an AGN jet base). However, jets can be loaded by protons following an interchange instabilities operating at the interface between the central (relativistic) and the external (non-relativistic) outflows. If both these outflows are Poynting flux dominated, then only the non-relativistic one is efficiently self-collimated. Therefore the two outflows press against each other resulting in mass exchange. Additionally, both the components are subject to kink (and other types of MHD) instabilities, which can increase the mass exchange rate. Unfortunately, no quantitative model exists to show whether efficient proton loading can be provided in this way. An alternative possibility is that the central, relativistic outflow is launched by the innermost portions of an accretion disc. Since the disc's parameters in the very central region depend strongly on the black hole spin, it is possible that the dependence of a jet power on the black hole spin is simply due to larger efficiency of a jet production in the case of a matter accreting onto rapidly rotating black hole. As pointed out by Sikora et al. (2005), also in this case the central portion of a jet can be relativistic, provided magnetic field lines are at small angles to the disc axis.

*(iii) Neutron star XRBs:* The discovery of relativistic jets in XRB systems with neutron stars proves that the existence of an ergosphere, which plays a key role in an extraction of a black hole rotational energy, is not necessary for producing relativistic jets. Does it contradict the proposed

spin paradigm? Let us recall that the condition for launching a Poynting-flux dominated outflow, which later becomes converted to a matter dominated relativistic jet, is to supply a high magnetic-to-rest-mass energy ratio ( $\gg 1$ ) at the base of the outflow. But this condition is obviously satisfied in the case of the magnetic field anchored on a neutron star. Moreover, as in the black-hole systems, slower winds from the accretion disc can collimate the central portion of the outflow launched from the rotating neutron star. Such a scenario provides a natural explanation for an abrupt drop of jet radio luminosities in neutron star XRBs below a certain X-ray luminosity (see Fig.3 in Migliari & Fender 2006): since the magnetic field anchored on a neutron star does not depend on the accretion rate, while the magnetic field in the disc does, the collimation of the outflow from a neutron star by a wind from the disc breaks below a given accretion rate. Of course, the lower the neutron-star magnetic field, the lower the accretion luminosity at the break, which can explain why millisecond accreting XRB pulsars are detected in radio even at very low accretion luminosities (see Fig.2 in Migliari & Fender 2006).

## 5. Conclusions

The main conclusions of our studies are:

- the upper boundaries of radio-loudness of AGNs hosted by giant elliptical galaxies are by  $\sim 3$  orders of magnitude larger than upper boundaries of radio-loudness of AGNs hosted by disc galaxies;
- both populations of spiral-hosted and elliptical-hosted AGNs show a similar dependence of the upper bounds of the radio loudness parameter  $\mathcal{R}$  on the Eddington ratio  $\lambda$ : the radio loudness increases with decreasing Eddington ratio, faster at higher accretion rates, slower at lower accretion rates;
- the huge, host-morphology-related difference between the radio-loudness reachable by AGNs in disc and elliptical galaxies can be explained by the scenario according to which
  - (i). the spin of a black hole determines the outflow’s power (in neutron star XRBs it is the neutron star rotation),
  - (ii). central black holes can reach large spins only in early type galaxies (following major mergers), and not (in a statistical sense) in spiral galaxies;
- a broad, “bottom-heavy” distribution of radio-loudness in quasars is not related to the distribution of the spin; however, it is still the BH spin which mediates launching of the jet and determines upper bound on the radio-loudness, whereas the interruptions in the jet production is suggested to be caused by intermittency of a jet collimation by MHD winds from the accretion disk.



### Acknowledgments

M.S. was partially supported by Polish MEiN grant 1 P03D 00928 and in 2005 by a CNRS “poste rouge” at IAP. L.S. acknowledges support by the MEiN grant 1 P03D 00329 and by the ENIGMA Network through the grant HPRN-CT-2002-00321. L.S. thanks the Fellows of the IAP for their hospitality and support during his stays there. JPL was supported in part by a grant from the CNES. He thanks the participants of the KITP program “Physics of Galactic Nuclei” for helpful remarks on the first version of this paper. We would like to thank Greg Madejski for his valuable comments which helped to improve the paper. We thank Jack Sulentic for pointing out an error in one of the tables. This project was partially supported by the Department of Energy contract to SLAC no. DE-AC3-76SF00515.

### REFERENCES

- Bardeen, J.M., & Petterson, J.A. 1975, *ApJ*, 195, L65
- Becker, R.H., White, R.L., & Edwards, A.L. 1991, *ApJS*, 75, 1
- Becker, R.H., White, R.L., & Helfand, D.J. 1995, *ApJ*, 450, 559
- Beckwith, K., & Done, C. 2004, *MNRAS*, 352, 353
- Begelman, M.C., & Li, Z.-Y. 1994, *ApJ*, 426, 269
- Beskin, V.S., & Nokhrina, E.E. 2006, *MNRAS*, 367, 375
- Blandford, R.D. 1990, in *Active Galactice Nuclei*, ed. T.J.-L. Courvoisier & M. Mayor (Saas-Fee Advanced Course 20)(Berlin:Spronger), 161
- Blandford, R.D., & Znajek, R.L. 1977, *MNRAS*, 179, 433
- Bogovalov, S., & Tsinganos, K. 2005, *MNRAS*, 357, 918
- Cao, X., & Rawlings, S. 2004, *MNRAS*, 349, 1419
- Capetti, A., Axon, D.J., Macchetto, F.D., et al. 1999, *ApJ*, 516, 187
- Chiaberge, M., Capetti, A., & Celotti, A. 1999, *A&A*, 349, 77
- Chiaberge, M., Capetti, A., & Macchetto, F.D. 2005, *ApJ*, 625, 716
- Cirasuolo, M., Magliocchrtti, M., Celotti, A., & Danese, L. 2003, *MNRAS*, 341, 993
- Cirasuolo, M., Celotti, A., Magliocchrtti, M., & Danese, L. 2003, *MNRAS*, 346, 447
- Condon, J.J., Cotton, W.D., Greissen, E.W., et al. 1998, *AJ*, 115, 1693

- Croom, S.M., Smith, R.J., Boyle, B.J., et al. 2001, MNRAS, 322, L29
- Done, C., & Gierliński, M. 2006, MNRAS, 367, 659
- Davis, S. W., Done, C., & Blaes, O. M. 2006, astro-ph/0602245
- Elvis, M., Risaliti, G., & Zamorani, G., 2002, ApJ, 565, L75
- Eracleous, M., & Halpern, J.P. 1994, ApJS, 90, 1
- Eracleous, M., & Halpern, J.P. 2003, ApJ, 599, 886
- Eracleous, M., & Halpern, J.P. 2004, ApJS, 150, 181
- Feigelson, E.D., Maccacaro, T., & Zamorani, G. 1982, ApJ, 255, 392
- Fender, R.P. 2004, astro-ph/030339
- Fender, R.P., Belloni, T.M., & Gallo, E. 2004, MNRAS, 355, 1105
- Fender, R., Wu, K., Johnston, H., et al. 2004, Nature, 427, 222
- Ferruit, P., Wilson, A. S., & Mulchaey, J. 2000, ApJS, 128, 139
- Floyd, D.J.E., Kukula, M.J., Dunlop, J.S., et al. 2004, MNRAS, 355, 196
- Fomalont, E.B., Geldzahler, B.J., & Bradshaw, C.F. 2001, ApJ, 558, 283
- Gallo, E., Fender, R.P., & Pooley, G.G. 2003, MNRAS, 344, 60
- Gracia, J., Tsinganos, K., & Bogovalov, S.V. 2005, A&A, 442, L7
- Gregory, P.C., & Condon, J.J. 1991, ApJS, 75, 1011
- Haas, M., Müller, S.A.H., Bertoldi, F., et al. 2004, A&A, 424, 531
- Hawley, J.F., & Krolik, J.H. 2006, ApJ, 641, 103
- Ho, L.C. 1999, ApJ, 516, 672
- Ho, L.C. 2002, ApJ, 564, 120
- Ho, L.C., & Peng, C.Y. 2001, ApJ, 555, 650
- Homan, D.C., Attridge, J.M., & Wardle, J.F.C. 2001, ApJ, 556, 113
- Hopkins, P.F., Bundy, K., Hernquist, L., & Ellis, R.S. 2006, ApJ, submitted (astro-ph/0601621)
- Hopkins, P.F., & Hernquist, L. 2006, astro-ph/0603180
- Hughes, S.A., & Blandford, R.D. 2003, ApJ, 585, L101

- Ivezić, Ž, Menou, K., Knapp, G.R., et al. 2002, AJ, 124, 2364
- Kellermann, K.I., Sramek, R., Schmidt, M., et al. 1989, AJ, 98, 1195
- Kharb, P., O’Dea, C.P., Baum, S.A., et al. 2006, astro-ph/0607603
- Kharb, P., & Shastri, P. 2004, A&A, 425, 825
- King, A.R., Lubow, S.H., Ogilvie, G.I., & Pringle, J.E. 2005, MNRAS, 363, 49
- Kinney, A.L., Schmitt, H.R., Clarke, C.J., et al. 2000, ApJ, 537, 152
- Knapp, G.R., Bies, W.E., & van Gorkom, J.H. 1990, AJ, 99, 476
- Komossa, S., Voges, W., Xu, D., et al. 2006, AJ, 132, 531
- Kühr, H., Witzel, A., Pauliny-Toth, I.I.K., & Nauber, U. 1981, A&AS, 45, 367
- Laor, A., 2003, ApJ, 590, 86
- Ledlow, M.J., Owen, F.N., Yun, M.S, & Hill, J.M. 2001, ApJ, 552, 120
- Livio, M., Pringle, J.E., & King, A.R. 2003, ApJ, 593, 184
- Lodato, G., & Pringle, J.E. 2006, MNRAS, 368, 1196
- Mapelli, M., Ferrara, A., & Rea, N. 2006, MNRAS, 368, 1340
- Marconi, A., Risaliti, G., Gilli, R., et al. 2004, MNRAS, 351, 169
- Mayer, M., & Pringle, J.E. 2006, MNRAS, 368, 379
- McHardy, I. M., Gunn, K. F., Uttley, P., & Goad, M. R. 2005, MNRAS, 359, 1469
- McKinney, J.C. 2006, MNRAS, 368, 1561
- McLure, R.J., & Jarvis, M.J. 2004, MNRAS, 353, L45
- Merloni, A., Heinz, S., & Di Matteo, T. 2003, MNRAS, 345, 1057
- Migliari, S., & Fender, R.P. 2006, MNRAS, 366, 79
- Miller, L., Peacock, J.A., & Mead, A.R.G. 1990, MNRAS, 244, 207
- Moderski, R., & Sikora, M. 1996a, MNRAS, 283, 854
- Moderski, R., & Sikora, M. 1996b, A&AS, 120C, 591
- Moderski, R., Sikora, M., & Lasota, J.-P. 1998, MNRAS, 301, 142
- Müller, S.A.H., Haas, M., Siebenmorgen, R., et al. 2004, A&A, 426, L29

- Nagar, N.M., Falcke, H., & Wilson, A.S. 2005, *A&A*, 435, 521
- Natarajan, P., & Pringle, J.E. 1998, *ApJ*, 506, L97
- Nipoti, C., Blundell, K.M., & Binney, J. 2005, *MNRAS*, 361, 633
- Papaloizou, J.C.B., & Pringle, J.E. 1983, *MNRAS*, 202, 1181
- Pedlar, A., Ghataure, H.S., Davies, R.D., et al. 1990, *MNRAS*, 246, 477
- Rees, M.J. 1978, *Nature*, 275, 516
- Richards, G.T., Lacy, M., Storrie-Lombardi, L.J., et al. 2006, *astro-ph/0601558*
- Sandage, A. 1965, *ApJ*, 141, 1560
- Schmidt, M., & Green, R.F., 1983, *ApJ*, 269, 352
- Schmitt, H.R., Antonucci, R.R.J., Ulvestad, J.S., et al. 2001, *ApJ*, 555, 663
- Shafee, R., McClintock, J. E., Narayan, R., Davis, S. W., Li, L.-X., & Remillard, R. A. 2006, *ApJ*, 636, L113
- Sikora, M., Begelman, M.C., Madejski, G.M., & Lasota, J.-P. 2005, *ApJ*, 625, 72
- Sikora, M., & Madejski, G.M. 2000, *ApJ*, 534, 109
- Sol, H., Pelletier, G., & Asseo, E. 1989, *MNRAS*, 237, 411
- Soltan, A. 1982, *MNRAS*, 200, 115
- Spruit, H.C., & Uzdensky, D.A. 2005, *ApJ*, 629, 960
- Stoeke, J.T., Morris, S.L., Weymann, R.J., et al. 1992, *ApJ*, 396, 487
- Strateva, I.V., Strauss, M.A., Hao, L., et al. 2003, *AJ*, 126, 1720
- Strittmatter, P.A., Hill, P., Pauliny-Toth, I.I.K., et al. 1980, *A&A*, 1980, 88, L12
- Terashima, Y., & Wilson, A.S. 2003, *ApJ*, 583, 145
- Tully, R.B., 1988, *Nearby Galaxies Catalog* (Cambridge: Cambridge Univ. Press)
- Ulvestad, J.S., Antonucci, R.R.J., & Goodrich, R.W. 1995, *AJ*, 109, 81
- Verdoes Kleijn, G.A., Baum, S.A., de Zeeuw, P.T. 2002, *AJ*, 123, 1334
- Véron-Cetti, M.-P., & Véron, P. 1989, *ESO Scientific Rep. No. 7, A Catalog of Quasars and Active Nuclei* (4th ed.; München: ESO)

- Véron-Cetti, M.-P., & Véron, P. 2001, *A&A*, 375, 791
- Vestergaard, M. 2002, *ApJ*, 571, 733
- Volonteri, M., Madau, P., Quataert, E., & Rees, M.J. 2005, *ApJ*, 620, 69
- Wardle, J.F.C., Homan, D.C., Ojha, R., et al. 1998, *Nature*, 395, 457
- Whalen, D.J., Laurent-Muehleisen, S.A., Moran, E.C., & Becker, R.H. 2006, *AJ*, 131, 1948
- White, R.L., & Becker, R.H. 1992, *ApJS*, 79, 331
- White, R.L., Becker, R.H., Gregg, M.D., et al. 2000, *ApJS*, 126, 133
- Wilms, J., Reynolds, C.S., Begelman, M.C., et al. 2001, *MNRAS*, 328, L27
- Wilson, A.S., & Colbert, E.J.M. 1995, *ApJ*, 438, 62
- Woo, J.-H., & Urry, C.M. 2002, *ApJ*, 579, 530
- Wright, A.E., Griffith, M.R., Burke, B.F., & Ekers, R.D. 1994, *ApJS*, 91, 111
- Wright, A.E., & Otrupcek, R. 1990, *Parkes Catalog 1990*, Australia Telescope National Facility
- Xu, C., Livio, M., Baum, S. 1999, *AJ*, 118, 1169
- Wu, X.-B., & Liu, F.K. 2004, *ApJ*, 614, 91
- York, D.G., Adelman, J., Anderson, J.E., Jr., et al. 2000, *AJ*, 120, 1579
- Yu, Q., & Tremaine, S. 2002, *MNRAS*, 335, 965
- Zhou, H. & Wang, T. 2002, *ChJAA*, 2, 501
- Zirbel, E.L., & Baum, S.A. 1995, *ApJ*, 448, 521

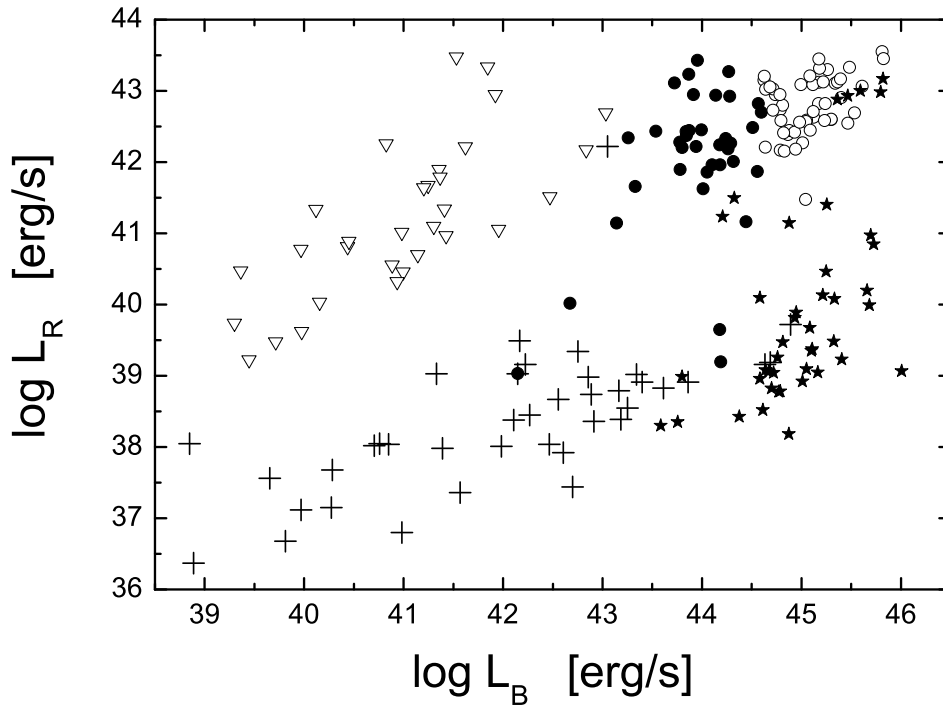


Fig. 1.— Total 5 GHz luminosity vs.  $B$ -band nuclear luminosity. BLRGs are marked by filled circles, radio-loud quasars by open circles, Seyfert galaxies and LINERS by crosses, FR I radio galaxies by open triangles, and PG Quasars by filled stars.

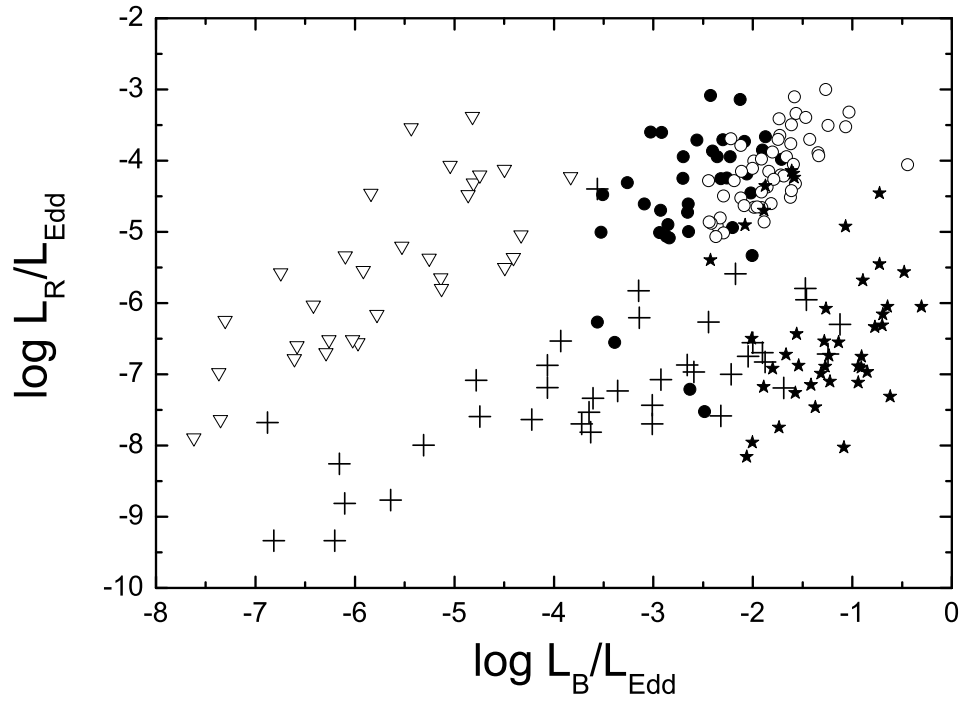


Fig. 2.— Total 5 GHz luminosity vs.  $B$ -band nuclear luminosity in the Eddington units. BLRGs are marked by the filled circles, radio-loud quasars by the open circles, Seyfert galaxies and LINERS by the crosses, FR I radio galaxies by the open triangles, and PG Quasars by the filled stars.

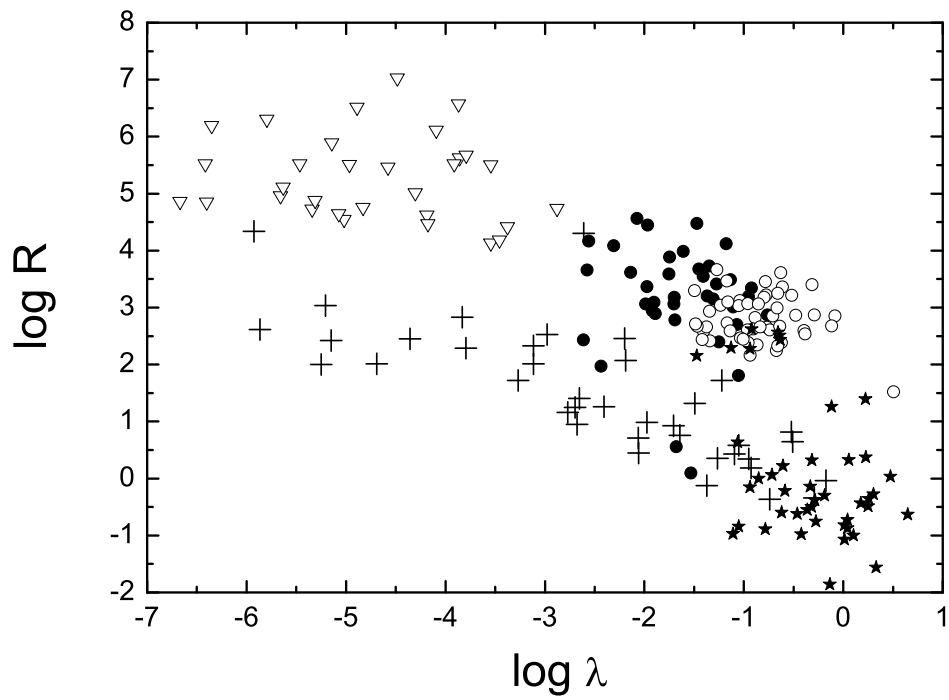


Fig. 3.— Radio-loudness  $\mathcal{R}$  vs. Eddington ratio  $\lambda$ . BLRGs are marked by the filled circles, radio-loud quasars by the open circles, Seyfert galaxies and LINERS by the crosses, FR I radio galaxies by the open triangles, and PG Quasars by the filled stars.



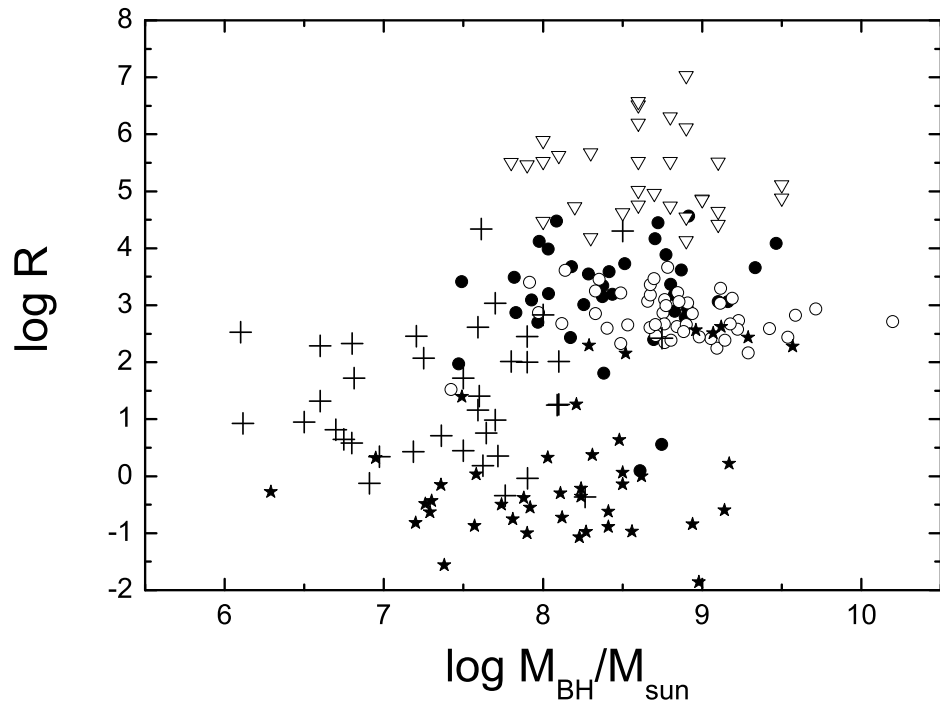


Fig. 4.— Radio-loudness vs. black hole mass. BLRGs are marked by the filled circles, radio-loud quasars by the open circles, Seyfert galaxies and LINERS by the crosses, FR I radio galaxies by the open triangles, and PG Quasars by the filled stars.

Table 1. Broad-Line Radio Galaxies

IAU J2000.0 (1)	name (2)	$z$ (3)	$m_V$ (4)	$A_V$ (5)	$\kappa_*$ (6)	$\log L_B$ [erg/s] (7)	$F_5$ [Jy] (8)	ref. to col. 8 (9)	$\log L_R$ [erg/s] (10)	$\log \mathcal{R}$ (11)	$FWHM_{H\alpha}$ [km/s] (12)	$\log \mathcal{M}_{BH}$ [ $M_\odot$ ] (13)	$\log L_B$ [ $L_{Edd}$ ] (14)	$\log L_R$ [ $L_{Edd}$ ] (15)
0038-0207	3C 17	0.22	18	0.08	0.58	43.9	2.48	1	43.2	4.45	11500	8.7	-2.9	-3.6
0044+1211	4C +11.06	0.226	19	0.26	0.28	43.8	0.22	1	42.2	3.49	4299	7.8	-2.1	-3.7
0207+2931	3C 59	0.11	16	0.21	0.28	44.4	0.67	2	42.0	2.78	9800	8.9	-2.6	-5.0
0224+2750	3C 67	0.311	18.6	0.42	0.82	43.8	0.87	2	43.1	4.48	6200	8.1	-2.4	-3.1
0238-3048	IRAS 02366-3101	0.062	15	0.22	0.3	44.2	0.00343	3	39.2	0.10	7800	8.6	-2.5	-7.5
0238+0233	PKS 0236+02	0.207	17.7	0.11	0.46	44.1	0.12	1	41.9	2.89	11200	8.8	-2.8	-5.1
0312+3916	B2 0309+39	0.161	18.2	0.49	0.1	44.0	0.822	2	42.5	3.55	6300	8.3	-2.4	-3.9
0342-3703	PKS 0340-37	0.285	18.6	0.03	0.19	44.2	0.71	1	42.9	3.89	9800	8.8	-2.7	-3.9
0343+0457	3C 93	0.357	19.2	0.8	0.43	44.3	0.91	1	43.3	4.09	19600	9.5	-3.3	-4.3
0452-1812	MS 0450.3-1817	0.059	17.8	0.14	0.9	42.2	0.0026	4	39.0	1.97	10900	7.5	-3.4	-6.6
0519-4546	Pictor A	0.035	16.2	0.14	0.14	43.3	15.54	5	42.3	4.17	18400	8.7	-3.5	-4.5
0832+3707	CBS 74	0.092	16	0.12	0.17	44.2	0.00424	6	39.6	0.56	9200	8.7	-2.6	-7.2
0849+0949	PKS 0846+101	0.365	19.2	0.19	0.11	44.3	0.1	1	42.3	3.18	9600	8.8	-2.7	-4.6
0859-1922	PKS 0857-191	0.361	19.7	0.69	0	44.3	0.4	1	42.9	3.73	6500	8.5	-2.3	-3.7
0914+0507	4C +05.38	0.302	17.4	0.17	0.51	44.6	0.22	1	42.5	3.06	10600	9.1	-2.7	-4.7
0923-2135	PKS 0921-213	0.053	16.5	0.2	0.65	43.2	0.42	1	41.1	3.09	8300	7.9	-2.9	-4.9
0947+0725	3C 227	0.086	16.3	0.09	0.4	43.9	2.6	1	42.4	3.62	13900	8.9	-3.1	-4.6
1030+3102	B2 1028+31	0.178	16.7	0.27	0.18	44.6	0.172	2	41.9	2.40	6400	8.7	-2.2	-4.9
1154-3505	PKS 1151-34	0.258	17.8	0.28	0.75	44.0	2.74	1	43.4	4.56	13400	8.9	-3.0	-3.6
1257-3334	PKS 1254-333	0.19	18.6	0.28	0.22	43.9	0.54	1	42.4	3.68	6300	8.2	-2.4	-3.9
1332+0200	3C 287.1	0.216	18.3	0.08	0.36	44.0	1.35	1	43.0	4.12	4700	8.0	-2.1	-3.1
1407+2827	Mrk 0668	0.077	15.4	0.06	0.27	44.2	2.421	2	42.2	3.15	6000	8.4	-2.3	-4.2
1419-1928	PKS 1417-19	0.12	16.7	0.28	0.05	44.3	0.83	1	42.2	3.01	4900	8.3	-2.1	-4.2
1443+5201	3C 303	0.141	17.3	0.06	0.73	43.6	1.044	2	42.4	3.99	6800	8.0	-2.6	-3.7
1516+0015	PKS 1514+00	0.053	15.6	0.18	0.76	43.4	1.37	1	41.7	3.42	4300	7.5	-2.2	-3.9
1533+3544	4C +35.37	0.157	17.8	0.08	0	44.1	0.129	2	41.6	2.70	4300	8.0	-2.0	-4.5
1617-3222	3C 332	0.151	16	0.08	0.85	43.9	0.92	2	42.4	3.66	23200	9.3	-3.5	-5.0
1637+1149	MC2 1635+119	0.147	16.5	0.17	0.14	44.5	0.051	2	41.2	1.81	4900	8.4	-2.0	-5.3
1719+4858	Arp 102B	0.024	14.8	0.08	0.86	42.7	0.159	2	40.0	2.43	16000	8.2	-3.6	-6.3
1742+1827	PKS 1739+184	0.186	17.5	0.21	0.11	44.3	0.39	1	42.3	3.06	13600	9.2	-2.9	-5.0
1835+3241	3C 382	0.058	15.4	0.23	0.06	44.1	2.281	2	42.0	2.95	11800	8.9	-2.9	-5.1
1842+7946	3C 390.3	0.056	15.4	0.24	0.31	44.0	4.45	5	42.2	3.37	11900	8.8	-2.9	-4.7
2101-4219	PKS 2058-425	0.223	17.2	0.13	0	44.6	0.71	1	42.7	3.19	4600	8.4	-1.9	-3.8
2223-0206	3C 445	0.056	15.8	0.27	0.33	43.8	2.12	1	41.9	3.20	5600	8.0	-2.3	-4.3
2303-1841	PKS 2300-18	0.129	17.8	0.11	0.14	43.8	0.89	1	42.3	3.59	8700	8.4	-2.7	-4.2

Table 1—Continued

IAU J2000.0 (1)	name (2)	$z$ (3)	$m_V$ (4)	$A_V$ (5)	$\kappa_*$ (6)	$\log L_B$ [erg/s] (7)	$F_5$ [Jy] (8)	ref. to col. 8 (9)	$\log L_R$ [erg/s] (10)	$\log \mathcal{R}$ (11)	$FWHM_{H\alpha}$ [km/s] (12)	$\log \mathcal{M}_{BH}$ [ $\mathcal{M}_\odot$ ] (13)	$\log L_B$ [ $L_{Edd}$ ] (14)	$\log L_R$ [ $L_{Edd}$ ] (15)
2307+1901	PKS 2305+188	0.313	17.5	0.44	0.56	44.6	0.44	1	42.8	3.34	4400	8.4	-1.9	-3.7
2330+1702	MC3 2328+167	0.28	18.3	0.15	0.37	44.2	0.078	2	42.0	2.87	3200	7.8	-1.7	-4.0

Note. — Reference in column 9: [1] Wright & Otrupcek (1990), [2] Gregory & Condon (1991), [3] Condon et al. (1998), [4] Feigelson et al. (1982), [5] Kuhr et al. (1981), [6] Becker et al. (1995), [7] Wright et al. (1994), [8] Becker et al. (1991).

Table 2. Radio-Loud Quasars

IAU J2000.0 (1)	name (2)	$z$ (3)	$m_V$ (4)	$A_V$ (5)	$\kappa_*$ (6)	$\log L_B$ [erg/s] (7)	$F_5$ [Jy] (8)	ref. to col. 8 (9)	$\log L_R$ [erg/s] (10)	$\log \mathcal{R}$ (11)	$FWHM_{H\alpha}$ [km/s] (12)	$\log \mathcal{M}_{BH}$ [ $\mathcal{M}_\odot$ ] (13)	$\log L_B$ [ $L_{Edd}$ ] (14)	$\log L_R$ [ $L_{Edd}$ ] (15)
0019+2602	4C 25.01	0.284	15.4	0.1	0	45.6	0.405	2	42.7	2.24	4600	9.1	-1.6	-4.5
0113+2958	B2 0110+29	0.363	17	0.21	0	45.2	0.311	2	42.8	2.73	7200	9.2	-2.1	-4.5
0157+3154	4C 31.06	0.373	18	0.18	0.11	44.8	0.394	2	43.0	3.30	9000	9.1	-2.4	-4.3
0202-7620	PKS 0202-76	0.389	16.9	0.17	0	45.3	0.8	1	43.3	3.12	6400	9.2	-2.0	-4.0
0217+1104	PKS 0214+10	0.408	17	0.36	0.01	45.4	0.46	1	43.1	2.85	4500	8.9	-1.7	-3.9
0311-7651	PKS 0312-77	0.225	16.1	0.32	0	45.2	0.59	1	42.6	2.59	2900	8.4	-1.3	-3.9
0418+3801	3C 111	0.049	18	5.46	0.04	45.1	6.637	2	42.3	2.35	4800	8.8	-1.8	-4.6
0559-5026	PKS 0558-504	0.138	15	0.15	0	45.1	0.121	7	41.5	1.52	1000	7.4	-0.4	-4.1
0745+3142	B2 0742+31	0.462	16	0.23	0	45.9	0.957	2	43.5	2.82	6500	9.6	-1.8	-4.2
0815+0155	PKS 0812+02	0.402	17.1	0.1	0.01	45.2	0.77	1	43.3	3.22	4600	8.8	-1.7	-3.6
0839-1214	3C 206	0.197	15.8	0.15	0	45.1	0.72	1	42.6	2.63	5100	8.8	-1.9	-4.4
0927-2034	PKS 0925-203	0.347	16.4	0.19	0	45.4	0.7	1	43.1	2.85	2200	8.3	-1.0	-3.3
0954+0929	4C +09.35	0.298	17.2	0.11	0	44.9	0.18	1	42.4	2.61	5100	8.7	-1.9	-4.4
1006-4136	PKS 1004-217	0.33	16.9	0.2	0	45.2	0.3	1	42.7	2.68	2100	8.1	-1.1	-3.5
1007+1248	PKS 1004+13	0.24	15.2	0.13	0	45.5	0.42	1	42.5	2.16	6100	9.3	-1.9	-4.9
1013-2831	PKS 1011-282	0.255	16.9	0.21	0	44.9	0.29	1	42.4	2.65	4100	8.5	-1.7	-4.2
1022-1037	PKS 1020-103	0.197	16.1	0.15	0	45.0	0.49	1	42.4	2.58	8700	9.2	-2.4	-4.9
1051-0918	3C 246	0.345	16.8	0.14	0	45.2	0.7	1	43.1	3.03	6300	9.1	-2.0	-4.1
1103-3251	PKS 1101-325	0.355	16.5	0.31	0	45.4	0.73	2	43.2	2.86	3500	8.8	-1.4	-3.7
1107+3616	B2 1104+36	0.392	18	0.06	0	44.8	0.217	2	42.7	3.04	6800	8.9	-2.2	-4.3
1131+3114	B2 1128+31	0.29	16	0.07	0.01	45.3	0.31	1	42.6	2.39	4000	8.8	-1.6	-4.3
1148-0404	PKS 1146-037	0.341	16.9	0.11	0.5	44.9	0.34	2	42.8	3.07	5000	8.7	-1.9	-4.0
1153+4931	LB 2136	0.333	17.1	0.07	0	45.0	0.702	2	43.1	3.18	4400	8.7	-1.7	-3.7
1159+2106	TXS 1156+213	0.347	17.5	0.09	0.43	44.7	0.085	2	42.2	2.66	7600	8.9	-2.3	-4.8
1210+3157	B2 1208+32A	0.389	16.7	0.06	0	45.3	0.16	2	42.6	2.39	5900	9.1	-1.9	-4.7
1225+2458	B2 1223+25	0.268	17.1	0.07	0	44.8	0.138	2	42.2	2.47	5400	8.7	-2.0	-4.7
1235-2512	PKS 1233-24	0.355	17.2	0.32	0	45.2	0.61	1	43.1	3.06	4900	8.9	-1.8	-3.9
1252+5624	3C 277.1	0.32	17.9	0.04	0	44.7	0.883	2	43.1	3.61	3200	8.1	-1.6	-3.1
1305-1033	PKS 1302-102	0.278	15.2	0.14	0	45.7	1	1	43.1	2.54	3400	8.9	-1.3	-3.9
1349-1132	PKS 1346-112	0.341	18	0.21	0	44.8	0.58	1	43.0	3.40	2300	7.9	-1.3	-3.0
1353+2631	B2 1351+26	0.308	17.2	0.05	0.1	44.9	0.098	2	42.2	2.42	7800	9.1	-2.3	-5.0
1359-4152	PKS 1355-41	0.314	15.9	0.29	0.05	45.5	1.4	1	43.3	2.93	9800	9.7	-2.3	-4.5
1423-5055	CSO 0643	0.276	16.7	0.04	0.28	44.9	0.225	2	42.4	2.68	9000	9.2	-2.4	-4.9
1454-3747	PKS 1451-375	0.314	16.7	0.26	0	45.2	1.84	1	43.4	3.36	3800	8.7	-1.6	-3.3
1514+3650	4C +37.43	0.371	16.3	0.07	0.04	45.4	0.361	2	42.9	2.59	7500	9.4	-2.1	-4.6

Table 2—Continued

IAU J2000.0 (1)	name (2)	$z$ (3)	$m_V$ (4)	$A_V$ (5)	$\kappa_*$ (6)	$\log L_B$ [erg/s] (7)	$F_5$ [Jy] (8)	ref. to col. 8 (9)	$\log L_R$ [erg/s] (10)	$\log \mathcal{R}$ (11)	$FWHM_{H\alpha}$ [km/s] (12)	$\log \mathcal{M}_{BH}$ [ $\mathcal{M}_\odot$ ] (13)	$\log L_B$ [ $L_{Edd}$ ] (14)	$\log L_R$ [ $L_{Edd}$ ] (15)
1527+2233	LB 9743	0.254	16.7	0.18	0	45.0	0.16	2	42.2	2.33	3700	8.5	-1.6	-4.4
1609+1756	4C + 18.47	0.346	18	0.18	0	44.8	0.28	1	42.7	3.10	6100	8.8	-2.1	-4.2
1704+6044	3C 351	0.372	15.3	0.08	0	45.9	1.258	2	43.5	2.71	13000	10.2	-2.4	-4.9
1721+3542	B2 1719+35	0.283	17.5	0.14	0.14	44.7	0.877	2	43.0	3.47	6000	8.7	-2.1	-3.8
1723+3417	B2 1721+34	0.205	16.5	0.12	0	44.8	0.65	2	42.6	2.87	2300	8.0	-1.2	-3.5
1728+0427	PKS 1725+044	0.297	17	0.47	0	45.1	1.21	1	43.2	3.21	3300	8.5	-1.5	-3.4
1748+1619	MRC 1745+163	0.392	17.6	0.31	0	45.1	0.146	2	42.6	2.61	4200	8.7	-1.7	-4.2
1917-4530	PKS 1914-45	0.364	16.8	0.27	0.1	45.3	0.18	1	42.6	2.44	9800	9.5	-2.4	-5.1
2142-0437	PKS 2140-048	0.345	18	0.11	0	44.7	0.6	1	43.1	3.46	3900	8.4	-1.7	-3.4
2143+1743	OX +169	0.211	15.7	0.37	0.01	45.3	1.061	8	42.8	2.67	4000	8.8	-1.6	-4.1
2211-1328	PKS 2208-137	0.391	17	0.15	0	45.3	0.53	1	43.1	2.99	4100	8.8	-1.6	-3.8
2230-3942	PKS 2227-399	0.318	17.9	0.06	0	44.7	1.02	1	43.2	3.67	6700	8.8	-2.2	-3.7
2250+1419	PKS 2247+14	0.235	16.9	0.17	0	44.8	1.11	1	42.9	3.25	3500	8.3	-1.6	-3.5
2305-7103	PKS 2302-713	0.384	17.5	0.1	0	45.0	0.15	1	42.6	2.66	4600	8.7	-1.8	-4.3
2351-0109	PKS 2349-01	0.174	15.3	0.09	0.05	45.1	0.68	1	42.4	2.44	5800	9.0	-2.0	-4.6

Note. — Reference in column 9: [1] Wright & Otrupcek (1990), [2] Gregory & Condon (1991), [3] Condon et al. (1998), [4] Feigelson et al. (1982), [5] Kuhr et al. (1981), [6] Becker et al. (1995), [7] Wright et al. (1994), [8] Becker et al. (1991).

Table 3. Seyfert Galaxies and Liners

IAU J2000.0 (1)	name (2)	$d$ [Mpc] (3)	$ M_B $ (4)	$\log L_B$ [erg/s] (5)	$\log L_R$ [erg/s] (6)	$\log \mathcal{R}$ (7)	$\log \mathcal{M}_{\text{BH}}$ [ $M_\odot$ ] (8)	ref. to col. 8 (9)	$\log L_B$ [ $L_{\text{Edd}}$ ] (10)	$\log L_R$ [ $L_{\text{Edd}}$ ] (11)
0006+2012	Mrk 335	114.2	18.33	42.9	38.4	0.58	6.8	1	-2.0	-6.6
0123-5848	Fairall 9	214.1	23.28	44.9	39.7	-0.04	7.9	1	-1.1	-6.3
0214-0046	Mrk 590	117.0	16.61	42.2	39.2	2.07	7.3	1	-3.1	-6.2
0242-0000	NGC 1068	14.4	16.47	42.2	39.5	2.46	7.2	1	-3.2	-5.8
0319+4130	NGC 1275	75.1	18.68	43.1	42.2	4.30	8.5	2	-3.6	-4.4
0516-0008	Ark 120	144.2	22.77	44.7	39.2	-0.36	8.3	1	-1.7	-7.2
0742+4948	Mrk 79	97.8	20.08	43.6	38.8	0.35	7.7	1	-2.2	-7.0
0919+6912	NGC 2787	7.5	8.27	38.9	36.4	2.62	7.6	1	-6.8	-9.3
0925+5217	Mrk 110	158.3	19.55	43.4	38.9	0.64	6.7	1	-1.5	-6.0
0955+6903	NGC 3031	3.9	11.73	40.3	37.1	2.01	7.8	1	-5.6	-8.8
1023+1951	NGC 3227	20.6	16.01	42.0	38.0	1.16	7.6	1	-3.7	-7.7
1106+7234	NGC 3516	38.9	17.21	42.5	38.0	0.71	7.4	1	-3.0	-7.4
1139+3154	Mrk 744	41.6	17.56	42.6	37.9	0.45	7.5	3	-3.0	-7.7
1139-3744	NGC 3783	38.5	19.01	43.2	38.4	0.34	7.0	–	-1.9	-6.7
1156+5507	NGC 3982	17.0	11.76	40.3	37.7	2.53	6.1	2	-3.9	-6.5
1157+5527	NGC 3998	14.1	12.95	40.8	38.0	2.42	8.7	1	-6.1	-8.8
1203+4431	NGC 4051	17.0	14.97	41.6	37.4	0.93	6.1	1	-2.7	-6.9
1210+3924	NGC 4151	20.3	19.18	43.3	38.5	0.43	7.2	1	-2.0	-6.7
1215+3311	NGC 4203	14.1	10.58	39.8	36.7	2.00	7.9	1	-6.2	-9.3
1218+2948	Mrk 766	55.4	16.72	42.3	38.4	1.32	6.6	4	-2.4	-6.3
1218+4718	NGC 4258	7.3	8.17	38.8	38.0	4.34	7.6	1	-6.9	-7.7
1225+1239	NGC 4388	16.8	13.17	40.8	38.0	2.33	6.8	4	-4.1	-6.9
1236+2559	NGC 4565	9.7	10.19	39.7	37.6	3.04	7.7	4	-6.2	-8.3
1237+1149	NGC 4579	16.8	12.81	40.7	38.0	2.45	7.9	4	-5.3	-8.0
1239-0520	NGC 4593	39.5	17.8	42.7	37.4	-0.13	6.9	1	-2.3	-7.6
1242+1315	NGC 4639	16.8	10.97	40.0	37.1	2.29	6.6	3	-4.7	-7.6
1313+3635	NGC 5033	18.7	14.53	41.4	38.0	1.72	7.5	3	-4.2	-7.6
1338+0432	NGC 5252	98.9	14.38	41.3	39.0	2.83	8.0	2	-4.8	-7.1
1342+3539	NGC 5273	21.3	13.51	41.0	36.8	0.95	6.5	2,3	-3.6	-7.8
1349-3018	IC 4329A	70.2	19.4	43.3	39.0	0.81	6.7	1	-1.5	-5.8
1353+6918	Mrk 279	135.6	20.7	43.9	38.9	0.18	7.6	1	-1.9	-6.8
1417+2508	NGC 5548	75.2	17.44	42.6	38.7	1.25	8.1	1	-3.6	-7.5
1436+5847	Mrk 817	140.4	18.96	43.2	38.8	0.76	7.6	1	-2.6	-7.0
1504+1026	Mrk 841	156.0	18.19	42.9	39.0	1.26	8.1	2	-3.4	-7.2
1531+0727	NGC 5940	145.2	18.27	42.9	38.7	0.99	7.7	2,3	-2.9	-7.1
1616+3542	NGC 6104	119.9	16.32	42.1	38.4	1.41	7.6	2	-3.6	-7.3
2044-1043	Mrk 509	154.1	22.63	44.6	39.2	-0.34	7.8	1	-1.2	-6.7
2303+0852	NGC 7469	71.4	17.93	42.8	39.3	1.72	6.8	1	-2.2	-5.6
2318+0014	Mrk 530	124.2	16.42	42.1	39.0	2.02	8.1	3	-4.1	-7.2

Note. — References in column 9: [1] Ho (2002), [2] Woo & Urry (2002), [3] Chiaberge et al. (2005), [4] Merloni et al. (2003).

Table 4. FR I Radio Galaxies

IAU J2000.0 (1)	name (2)	$z$ (3)	$\log L_B$ [erg/s] (4)	$F_5$ [Jy] (5)	ref. to col. 5 (6)	$\log L_R$ [erg/s] (7)	$\log \mathcal{R}$ (8)	$\log \mathcal{M}_{BH}$ [ $\mathcal{M}_\odot$ ] (9)	ref. to col. 9 (10)	$\log L_B$ [ $L_{Edd}$ ] (11)	$\log L_R$ [ $L_{Edd}$ ] (12)
0055+2624	3C 28	0.1952	<41.4	0.15	1	41.9	>5.63	8.1	1	<-4.8	-4.3
0057-0123	3C 29	0.0448	41.3	2.01	1	41.7	5.51	9.1	1	-5.9	-5.5
0057+3021	NGC 315	0.0167	41.0	0.914	2	40.5	4.55	8.9	2	-6.0	-6.6
0107+32224	3C 31	0.0169	40.9	1.12	2	40.6	4.76	8.6	1	-5.8	-6.2
0123+3315	NGC 507	0.0164	<39.5	0.055	3	39.2	>4.86	9	2	<-7.6	-7.9
0125-0120	3C 40	0.018	<40.5	1.78	1	40.8	>5.46	7.9	2	<-5.5	-5.2
0156+0537	NGC 741	0.0185	<40.2	0.28	1	40.0	>4.96	8.7	2	<-6.6	-6.8
0223+4259	3C 66B	0.0215	41.5	1.77	2	41.0	4.63	8.5	1	-5.1	-5.6
0308+0406	3C 78	0.0288	42.5	3.45	1	41.5	4.13	8.9	1	-4.5	-5.5
0318+4151	3C 83.1	0.0251	40.2	3.034	4	41.3	6.30	8.8	1	-6.7	-5.6
0319+4130	3C 84	0.0176	42.9	42.37	2	42.2	4.42	9.1	1	-4.3	-5.0
0334-0110	3C 89	0.1386	<40.9	0.72	1	42.3	>6.52	8.6	1	<-5.8	-4.5
1145+1936	3C 264	0.0206	42.0	2.36	1	41.1	4.18	8.3	1	-4.4	-5.4
1219+0549	3C 270	0.0074	39.4	4.86	1	40.5	6.20	8.6	1	-7.3	-6.2
1225+1253	3C 272.1	0.0037	40.0	2.72	1	39.6	4.73	8.2	1	-6.3	-6.7
1230+1223	3C 274	0.0037	41.0	67.6	1	41.0	5.12	9.5	1	-6.6	-6.6
1259+2757	NGC 4874	0.0239	<39.3	0.084	2	39.7	>5.52	8.6	2	<-7.4	-7.0
1338+3851	3C 288	0.246	42.0	1.008	2	42.9	6.11	8.9	1	-5.0	-4.1
1416+1048	3C 296	0.0237	40.5	1.202	2	40.9	5.52	8.8	1	-6.4	-6.0
1504+2600	3C 310	0.054	41.3	1.26	1	41.6	5.52	8	1	-4.9	-4.5
1510+7045	3C 314.1	0.1197	<41.4	0.337	2	41.8	>5.51	7.8	1	<-4.5	-4.1
1516+0701	3C 317	0.0342	41.4	0.93	1	41.1	4.88	9.5	1	-6.3	-6.5
1628+3933	3C 338	0.0303	41.2	0.477	2	40.7	4.65	9.1	1	-6.0	-6.5
1643+1715	3C 346	0.162	43.1	1.39	2	42.7	4.74	8.8	1	-3.8	-4.2
1651+0459	3C 348	0.154	41.6	9.529	2	43.5	7.03	8.9	1	-5.4	-3.5
2048+0701	4C 424	0.127	<41.7	0.785	2	42.2	>5.68	8.3	1	<-4.7	-4.2
2155+3800	3C 438	0.29	<41.9	1.703	2	43.3	>6.58	8.6	1	<-4.8	-3.4
2214+1350	3C 442	0.0262	40.0	0.76	1	40.8	5.89	8	1	-6.1	-5.3
2231+3921	3C 449	0.0181	41.0	0.566	2	40.3	4.47	8	1	-5.1	-5.8
2320+0813	NGC 7626	0.0113	<39.8	0.21	1	39.5	>4.85	9	2	<-7.4	-7.6
2338+2701	3C 465	0.0301	41.5	2.12	1	41.3	5.02	8.6	1	-5.3	-5.4

Note. — References in column 6: [1] Wright & Otrupcek (1990), [2] Gregory & Condon (1991), [3] White & Becker (1992), [4] Kuhr et al. (1981). References in column 10: [1] Cao & Rawlings (2004), [2] Woo & Urry (2002).

Table 5. PG Quasars

IAU J2000.0 (1)	name (2)	$z$ (3)	$\log L_B$ [erg/s] (4)	$F_5$ [Jy] (5)	$\log L_R$ [erg/s] (6)	$\log \mathcal{R}$ (7)	$\log \mathcal{M}_{BH}$ [ $\mathcal{M}_\odot$ ] (8)	ref. to col. 8 (9)	$\log L_B$ [ $L_{Edd}$ ] (10)	$\log L_R$ [ $L_{Edd}$ ] (11)
0010+1058	PG 0007+106	0.089	44.3	0.321	41.5	2.29	8.3	1	-2.1	-4.9
0029+1316	PG 0026+129	0.142	45.2	0.0051	40.1	0.03	7.6	2	-0.5	-5.6
0053+1241	PG 0050+124	0.061	44.7	0.0026	39.1	-0.48	7.3	1	-0.7	-6.3
0054+2525	PG 0052+251	0.155	45.1	7.4E-4	39.4	-0.62	8.4	2	-1.4	-7.1
0159+0023	PG 0157+001	0.164	45.2	0.008	40.5	0.33	8.0	1	-0.9	-5.7
0810+7602	PG 0804+761	0.1	44.8	0.00238	39.5	-0.22	8.2	2	-1.5	-6.9
0847+3445	PG 0844+349	0.064	44.9	3.1E-4	38.2	-1.56	7.4	2	-0.6	-7.3
0925+1954	PG 0923+201	0.19	45.0	2.5E-4	39.1	-0.84	8.9	2	-2.0	-8.0
0926+1244	PG 0923+129	0.029	43.8	0.01	39.0	0.32	7.0	1	-1.3	-6.1
0956+4115	PG 0953+414	0.239	45.7	0.0019	40.2	-0.36	8.2	2	-0.7	-6.2
1014+0033	PG 1012+008	0.185	45.1	1E-3	39.7	-0.30	8.1	1	-1.1	-6.6
1051-0051	PG 1049-005	0.357	45.7	4.8E-4	40.0	-0.60	9.1	1	-1.6	-7.3
1104+7658	PG 1100+772	0.313	45.6	0.66	43.0	2.51	9.1	1	-1.6	-4.2
1106-0052	PG 1103-006	0.425	45.8	0.482	43.2	2.44	9.3	1	-1.6	-4.2
1117+4413	PG 1114+445	0.144	44.8	2.2E-4	38.8	-0.89	8.4	1	-1.7	-7.7
1119+2119	PG 1116+215	0.177	45.3	0.0028	40.1	-0.14	8.5	1	-1.3	-6.5
1121+1144	PG 1119+120	0.049	44.4	9.4E-4	38.4	-0.82	7.2	1	-0.9	-6.9
1204+2754	PG 1202+28	0.165	45.3	8.3E-4	39.5	-0.73	8.1	1	-0.9	-6.8
1214+1403	PG 1211+143	0.085	44.9	0.157	41.1	1.39	7.5	2	-0.7	-4.5
1219+0638	PG 1216+069	0.334	45.7	0.004	40.8	0.22	9.2	1	-1.6	-6.4
1232+2009	PG 1229+204	0.064	44.6	6.7E-4	38.5	-0.97	8.6	2	-2.1	-8.2
1246+0222	PG 1244+026	0.048	43.8	8.3E-4	38.4	-0.28	6.3	1	-0.6	-6.1
1301+5902	PG 1259+593	0.472	46.0	3E-5	39.1	-1.86	9.0	1	-1.1	-8.0
1309+0819	PG 1307+085	0.155	45.2	3.5E-4	39.0	-1.00	7.9	2	-0.8	-7.0
1312+3515	PG 1309+355	0.184	45.3	0.054	41.4	1.26	8.2	1	-1.1	-4.9
1353+6345	PG 1351+640	0.087	44.6	0.0133	40.1	0.64	8.5	2	-2.0	-6.5
1354+1805	PG 1352+183	0.158	45.0	2.5E-4	38.9	-0.97	8.3	1	-1.4	-7.5
1405+2555	PG 1402+261	0.164	45.1	6.2E-4	39.4	-0.64	7.3	2	-0.3	-6.1
1413+4400	PG 1411+442	0.089	44.8	6.1E-4	38.8	-0.87	7.6	2	-0.9	-6.9
1417+4456	PG 1415+451	0.114	44.7	4E-4	38.8	-0.76	7.8	1	-1.2	-7.1
1419-1310	PG 1416-129	0.129	44.9	0.0036	39.9	0.06	8.5	1	-1.7	-6.7
1429+0117	PG 1426+015	0.086	44.7	0.00121	39.0	-0.55	7.9	2	-1.3	-7.0
1442+3526	PG 1440+356	0.077	44.6	0.00166	39.1	-0.44	7.3	1	-0.8	-6.3
1446+4035	PG 1444+407	0.267	45.4	1.6E-4	39.2	-1.07	8.2	1	-0.9	-7.1
1535+5754	PG 1534+580	0.03	43.6	0.00192	38.3	-0.16	7.4	1	-1.9	-7.2
1547+2052	PG 1545+210	0.266	45.4	0.72	42.9	2.62	9.1	1	-1.9	-4.4
1613+6543	PG 1613+658	0.129	44.9	0.00303	39.8	0	8.6	2	-1.8	-6.9
1620+1724	PG 1617+175	0.114	44.8	0.00109	39.3	-0.38	7.9	2	-1.2	-6.7
1701+5149	PG 1700+518	0.292	45.7	0.0072	41.0	0.37	8.3	2	-0.7	-5.5
2132+1008	PG 2130+099	0.061	44.6	0.00205	39.0	-0.50	7.7	2	-1.3	-6.9
2211+1841	PG 2209+184	0.07	44.2	0.29	41.2	2.15	8.5	1	-2.4	-5.4
2254+1136	PG 2251+113	0.323	45.5	0.523	42.9	2.56	9.0	1	-1.6	-4.1
2311+1008	PG 2308+098	0.432	45.8	0.303	43.0	2.27	9.6	1	-1.9	-4.7

Note. — References in column 9: [1] Vestergaard (2002), [2] Woo & Urry (2002).